Revealing hidden regularities with a general approach to fission

Karl-Heinz Schmidt [a] and Beatriz Jurado [b]

CENBG, CNRS/IN2P3, Chemin du Solarium B. P. 120, 33175 Gradignan, France

Abstract. Selected aspects of a general approach to nuclear fission are described with the focus on the possible benefit of meeting the increasing need of nuclear data for the existing and future emerging nuclear applications. The most prominent features of this approach are the evolution of quantum-mechanical wave functions in systems with complex shape, memory effects in the dynamics of stochastic processes, the influence of the Second Law of thermodynamics on the evolution of open systems in terms of statistical mechanics, and the topological properties of a continuous function in multi-dimensional space. It is demonstrated that this approach allows reproducing the measured fission barriers and the observed properties of the fission fragments and prompt neutrons Our approach is based on sound physical concepts, as demonstrated by the fact that practically all the parameters have a physical meaning, and reveals a high degree of regularity in the fission observables. Therefore, we expect a good predictive power within the region extending from Po isotopes to Sg isotopes where the model parameters have been adjusted. Our approach can be extended to other regions provided that there is enough empirical information available that allows determining appropriate values of the model parameters. Possibilities for combining this general approach with microscopic models are suggested. These are supposed to enhance the predictive power of the general approach and to help improving or adjusting the microscopic models. This could be a way to overcome the present difficulties for producing evaluations with the required accuracy.

PACS. 24.75.+i General properties of fission – 24.10.Pa Thermal and statistical models

1 Introduction

In the theory of nuclear fission, considerable progress has been made. The potential-energy surface of the fissioning systems has been systematically mapped in five-dimensional deformation space [1]. Stochastic methods [2–7] and self-consistent microscopic approaches [8,9] have been developed for dynamical calculations of low-energy fission. However, these calculations still face severe restrictions that are caused by limited computing power and by the lack of suitable theoretical formalisms. Generally, only a subset of the degrees of freedom of the fissioning system is considered. Moreover, the theoretical understanding of the fission process cannot fully rely on the powerful standard methods conceived for describing static nuclear properties; it still requires developing new methods for modelling non-equilibrium processes in nuclei, see *e.g.* [10–12].

Many attempts have been made to develop methods for describing the fission-fragment yields and other fission properties with the precision that is required for application in nuclear technology, the most comprehensive ones being coordinated by the International Atomic-Energy Agency (IAEA) [13,14]. They span the range from empirical compilations and evaluations over semi-empirical

systematics to theoretical models. Empirical descriptions have excellent quality for systems, for which reliable experimental data have been measured, but their predictive power for other fissioning systems or for other excitation energies is rather limited. There is presently considerable activity in this field, *e.g.* refs. [15–18]. Theoretical models are already very successful in describing general trends but fail to reproduce experimental data closely enough.

In this work we describe the main features of the GEneral Fission model (GEF), a semi-empirical approach that combines new experimental information, *e.g.* [19,20,?], with several long-standing [22,23] and some newly developed theoretical ideas [24,25]. This novel approach aims to unite a good reproduction of measured data with a high predictive power. A comprehensive documentation of the model can be found elsewhere [26].

The most important static property of the fissioning system is the deformation-dependent potential energy, in particular the height of the fission barrier. There is a great divergence in the theoretical predictions of fission barriers for exotic nuclei, *e.g.* those on the r-process path. But also the deviations from measured data exceed the experimental uncertainties appreciably. An important source of uncertainty is the difficulty in precisely calculating complex effects of nuclear structure. By making use of the topological properties of the potential-energy surface, these diffi-

---
[a] *E-mail:* schmidt-erzhausen@t-online.de
[b] *E-mail:* jurado@cenbg.in2p3.fr

culties are demonstrated, and possibilities are shown, how they can be overcome.

The description of fission observables, for example the properties of the fission fragments, is even more challenging, because it relies on the modelling of the dynamics of the fissionning system. Like most of the previous descriptions, which go beyond purely empirical compilations and evaluations of experimental data, the present work utilises the concept of independent fission channels [27, 28]. In the original Brosa model [28], the properties of the fission channels could not be predicted; they had to be determined for each fissioning system individually from experimental data, mostly from two-dimensional mass-yield - total-kinetic-energy distributions. Effort was invested to establish empirical systematics of the parameters of fission channels [29–31] or to deduce the fission-channel properties from shell-model calculations [32]. Our model follows a different approach, based on the separability [24] of macroscopic and microscopic properties on the fission path. According to the separability principle, the macroscopic potential-energy surface, dissipation and inertia are properties of the fissioning system, while the shell corrections in these quantities between the outer saddle and the scission point are essentially properties of the nascent fragments. Thus, to a good approximation the shell corrections are uniquely determined by the neutron and proton numbers of the two fission fragments, independently from the fissioning systems. This concept enables a consistent description of fission-fragment yields and other fission properties for a large range of fissioning nuclei with a very restricted set of parameters. In addition, most of the parameters of our model are directly related to physical quantities, like the height of the mass-asymmetry-dependent outer fission barrier, the shell-correction energy and the $\hbar\omega$ values of the normal modes beyond the outer barriers as well as the parameters of the energy-dependent level-densities for the different fission channels. This approach proves to be very successful for application in nuclear technology and for an improved understanding of some global aspects of nuclear fission.

The transformation of energy between potential energy, intrinsic and collective excitations as well as kinetic energy is another very important aspect of the nuclear-fission process. It determines the partition of the fission Q value (plus eventually the initial excitation energy of the fissioning system) between kinetic and excitation energy of the final fragments. Moreover, the division of the total excitation energy between the fragments is of considerable interest, because it induces a shift of the isotopic distributions from the primary fragments by neutron evaporation towards less neutron-rich isotopes. The present work takes advantage of the general laws of statistical mechanics to describe the energetics of the fissioning system. Statistical mechanics in particular requires that the available energy tends to be distributed among the accessible degrees of freedom in equal share during the dynamical evolution of the system. This general law provides an estimation of the evolution of the intrinsic excitation energies and the population of the available states in the nascent fragments during the fission process.

Possible ways are discussed, how the benefits of the present general approach and of microscopic models could be combined. While the general approach elucidates global trends and systematic variations of the fission observables and reproduces empirical data with a remarkable accuracy, microscopic models reduce the dependency from empirical data and improve the predictive power.

2 Fission barriers

During the last years, the efforts for developing improved models for the calculation of fission barriers were intensified, using the macroscopic-microscopic approach [33–39], the density-functional theory [40,41] and varieties of Hartree-Fock methods [42–46]. Still, the results from the different models, in particular in regions, where no experimental data exist, differ appreciably.

An alternative approach was used in ref. [48], by estimating the fission barrier as the difference of the macroscopic fission barrier B_f^{mac} and the ground-state shell correction δE_{gs}^{shell}, making use of the topographic theorem [23,49] that states that the shell correction δE_{sad}^{shell} at the barrier is negligeably small. The situation is illustrated in fig. 1.

Odd-even fluctuations due to pairing correlations need not to be considered, because they cancel, if one assumes that they are identical in the ground state and at the barrier. According to an elaborate analysis in [50], the average trend of the fission-barrier height along isotopic chains is very well reproduced by the Thomas-Fermi model of Myers and Swiatecki [23,51]. Therefore, the comprehensive set of empirical fission barriers from ref. [52] that are extracted from experimental fission probabilities and cross sections are compared in fig. 2 with the quantity

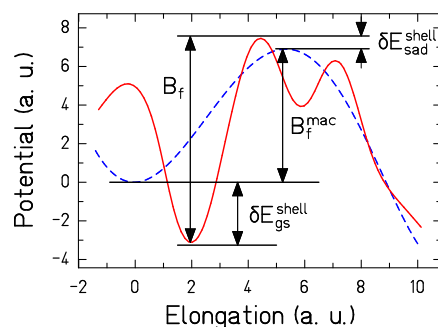$$B_f^{topo} = B_f^{TF} - E_{gs-nopair}^{exp} + E_{gs}^{TF} \qquad (1)$$

Fig. 1. Schematic drawing of the potential energy on the fission path relative to the macroscopic ground-state energy E_{gs}^{mac} for a nucleus that is deformed in its ground state. Spherical shape corresponds to zero elongation. Blue dashed line: macroscopic potential. Red full line: full potential including the shell effect.
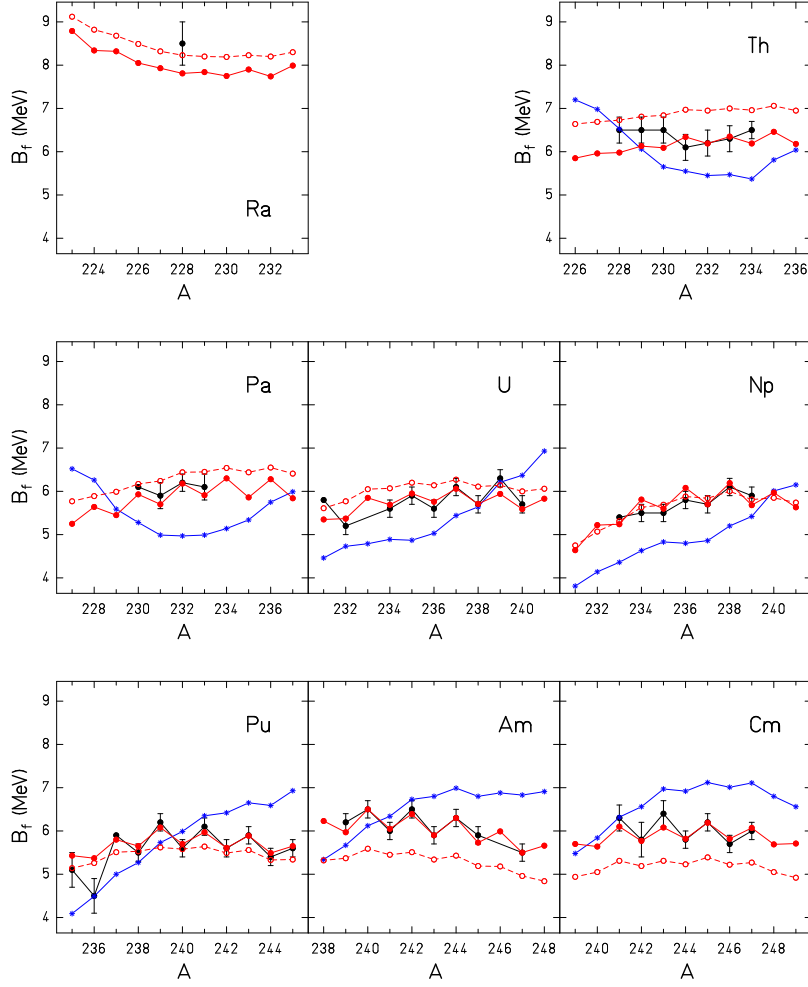
Fig. 2. The empirical fission threshold of ref. [52] (full black circles) is compared to the value (open red circles) estimated from the topographic theorem according to Eq. (1) for isotopic sequences of different elements. In addition, a modified estimation (full red circles) with a Z-dependent shift and an assumed increased pairing parameter $\Delta_f = 14/\sqrt{A}$ MeV at the barrier according to Eq. (2) as well as the theoretical prediction of the microscopic-macroscopic approach of ref. [35] (blue asterisks) are shown. Empirical values without error bars are given without an uncertainty range in ref. [52].
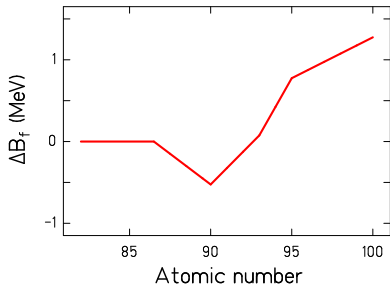

Fig. 3. Empirical correction applied to the fission-barrier height obtained with the topographical theorem as a function of the atomic number of the fissioning nucleus. The figure is taken from ref. [26].

where B_f^{TF} denotes the macroscopic fission barrier of ref. [51], represented by B_f^{mac} in fig. 1, and E_{gs}^{TF} is the macroscopic ground-state energy from the Thomas-Fermi model of ref. [23]. Both quantities do not contain neither shell nor pairing effects. $E_{gs-nopair}^{exp}$ was taken from the 2012 Atomic Mass Evaluation, averaged over odd-even fluctuations in Z and N. The quantity $E_{gs-nopair}^{exp} - E_{gs}^{TF}$ defines the empirical ground-state shell correction, represented by δE_{gs}^{shell} in fig. 1.

In accordance with ref. [50], the overall isotopic trend of the empirical barriers is rather well reproduced by B_f^{topo}, however, there are some systematic deviations: Firstly, the barriers of thorium, protactinium and uranium isotopes are overestimated, while the barriers of the heaviest elements plutonium, americium and curium are underestimated. Secondly, a systematic odd-even staggering that
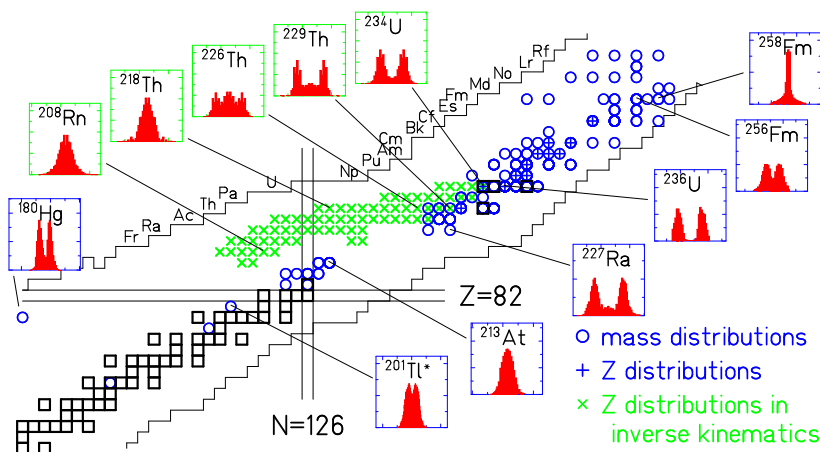
Fig. 4. General view on the systems for which mass or nuclear-charge distributions have been measured. The distributions are shown for 12 selected systems. Blue circles (blue crosses): Mass (nuclear-charge) distributions, measured in conventional experiments ([53,54], and references given in [19]). Green crosses: Nuclear-charge distributions, measured in inverse kinematics [19]. The figure is taken from ref. [55]. The shaded area indicates the domain of validity of the GEF code.

is evident in the empirical barriers from protactinium to curium is not reproduced by the B_f^{topo} values estimated with the topographic theorem.

A much better description of the barriers is obtained by applying a rather simple Z-dependent shift ΔB_f, shown in fig. 3 that compensates the average systematic deviations for the different isotopic sequences, and by assuming that the pairing-gap parameter at the barrier in protons and neutrons is increased with respect to the ground state. Best agreement is found by assuming $\Delta_f = 14$ MeV$/\sqrt{A}$, compared to the average value $\Delta_{gs} = 12$ MeV$/\sqrt{A}$ found in the ground-state masses. Thus the modified estimated barriers are given by

$$B_{f-mod}^{topo} = B_f^{TF} - E_{gs}^{exp} + E_{gs}^{TF} - n \cdot 14 \text{ MeV}/\sqrt{A} + \Delta B_f \quad (2)$$

E_{gs}^{exp} is the empirical ground-state energy, directly taken from the 2012 Atomic Mass Evaluation. Thus, it contains not only the shell effects, but also the odd-even staggering of the ground-state energies. n is 2 for even-even nuclei, 1 for odd-mass nuclei, and 0 for odd-odd nuclei. The Z-dependent shift ΔB_f is negative around thorium. The shift increases towards heavier elements and is assumed to vanish for lighter elements. Most of the B_{f-mod}^{topo} values lie inside the error bars of the empirical values that are typically 0.2 MeV. Note that the sum of macroscopic ground-state energy E_{gs}^{TF} and fission barrier height B_f^{TF} in eqs. (1) and (2) is equal to the fission-barrier energy (mass at the fission barrier in energy units):

$$E_f^{TF} = E_{gs}^{TF} + B_f^{TF}. \quad (3)$$

In addition, fig. 2 shows the predictions of an elaborate theoretical model [35] that is based on the microscopic-macroscopic approach from $Z = 90$ to $Z = 96$. The model values deviate appreciably from the empirical values. In

particular, the isotopic trend is not well reproduced. Moreover, the model does not show the observed odd-even fluctuations of the barrier height. This is rather discouraging, because the calculation relies on a meticulous mapping of the potential in five-dimensional deformation space [1].

3 Fission-fragment distributions

The observables from low-energy fission show strong manifestations of quantum-mechanical effects like the contributions of the different fission channels to the fission-fragment mass distributions that are related to nuclear shell effects and the considerable enhancement of even-Z fission fragments that are related to pairing correlations. These quantum-mechanical features are responsible for great part of the complexity of nuclear fission, and, thus, they considerably complicate the theoretical description of the fission process.

Figure 4 gives an overview on the measured mass and nuclear-charge distributions of fission products from low-energy fission. Fission of target nuclei in the actinide region, mostly induced by thermal neutrons, shows predominantly asymmetric mass splits. A transition to symmetric mass splits is seen around mass 258 in spontaneous fission of fusion residues. Electromagnetic-induced fission of relativistic secondary beams covers the transition from asymmetric to symmetric fission around mass 226 [19]. A pronounced fine structure close to symmetry appears in ^{201}Tl [53] and in ^{180}Hg [54]. It is difficult to observe low-energy fission in this mass range. Thus, ^{201}Tl could only be measured down to 7.3 MeV above the fission barrier due to its low fissility. This relatively high energy explains the filling of the minimum between the two peaks compared to ^{180}Hg that was measured at energies close to the barrier after beta decay of ^{180}Tl. Considering the measured energy dependence of the structure for ^{201}Tl [53],

the fission characteristics of these two nuclei are rather similar. Also other nuclei in this mass region show similar features, which have been attributed to the influence of fragment shells [56].

Let us first consider the different stages of the dynamical evolution of the fissioning system. At first, the nucleus needs to leave the first minimum at its ground-state shape, by passing the fission barrier, which in the actinides consists of two or more consecutive barriers with a minimum in between. Since tunneling proceeds with a very low probability, as can be deduced from the long spontaneous-fission half lives, an excited nucleus has enough time to rearrange its available energy. The probability for the passage of the fission barrier increases considerably, if the nucleus concentrates enough of its energy on the relevant shape degrees of freedom for avoiding tunneling as much as the available energy allows. The remaining energy, however, can be randomly distributed between the different states above the barrier without any further restriction, such that the barrier is passed with maximum possible entropy on the average [57]. For this reason, the fissioning system has no memory on the configurations before the barrier, except the quantities that are preserved due to general conservation laws: total energy, angular momentum and parity. Thus, the starting point of the model is the configuration above the outer fission barrier.

Beyond the outer barrier, one can define an optimum static fission path, consisting of a sequence of configurations in deformation space with minimum potential energy for a certain elongation. (The dynamic fission path will deviate from the static fission path due to the influence of dissipation and inertia.) This picture is helpful for revealing that the fissioning system is unbound only with respect to one degree of freedom, the motion in direction of the fission path. The system is bound with respect to motion in any other direction in deformation space. Some of the degrees of freedom of the system are directly linked to fission observables, *e.g.* the mass asymmetry $A_1/(A_1+A_2)$ or the charge polarisation $< Z_1 > -Z_{UCD}$. [1] with $Z_{UCD} = A_1 \cdot Z_{CN}/A_{CN}$. A_{CN} , Z_{CN} , A_i, and Z_i are mass and atomic number of the fissioning system and of one fragment, respectively. The fission-fragment distribution in Z and A is given by the evolution of the respective collective variables, until the system reaches the scission configuration. The value of the respective collective variable is the integral result of the forces acting on the whole fission path, including the influence of dissipation and inertial forces.

When the two-centre shell model became available, it was possible to study the single-particle structure in a di-nuclear potential with a necked-in shape. Investigations of Mosel and Schmitt [58] revealed that the single-particle structure in the vicinity of the outer fission barrier al-
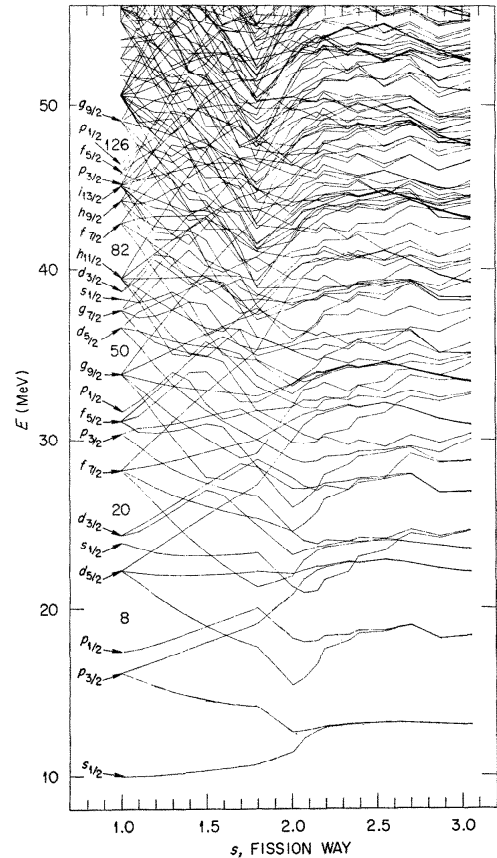
---

[1] For a continuous tracking of these degrees of freedom, suitable prescriptions must be defined that generalise these values that are defined for the separated fragments to the respective deformation parameters of the system on the fission path before scission. This is usually provided by the shape parameterisation.

Fig. 5. Neutron shell-model states calculated with the two-center shell model for the nucleus ^{236}U. The coordinate s characterizes the nuclear shape on the fission path. The figure covers the range from the spherical shape ($s = 1$) to a configuration with a neck radius of about 40 % of the maximum extension of the system perpendicular to the symmetry axis ($s \approx 3.1$). The outer saddle is located at $s = 1.7$. The figure is taken from ref. [58].

ready resembles very much the coherent superposition of the single-particle levels in the two separated fragments after fission. Figure 5 demonstrates that the single-particle energies remain almost constant little behind the outer saddle up to scission. The authors explained this result by the general quantum-mechanical feature that wave functions in a slightly necked-in potential are already essentially localized in the two parts of the system. Also recent self-consistent calculations show this feature (*e.g.* ref. [9]), which is a direct consequence of the necking, independent from the specific shape parameterisation. This finding immediately leads to the expectation that the shells on the fission path that are responsible for the complex structure of fission modes are essentially given by the fragment shells. Potential-energy surfaces of fissioning systems calculated with the macroscopic-microscopic approach (*e.g.* ref. [35] support this assumption.

As a consequence, the shell effects on the fission path can be approximately considered as the sum of the shell effects in the proton- and neutron-subsystems of the light
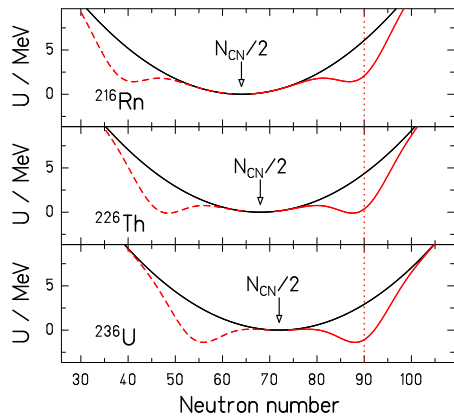
Fig. 6. Schematic illustration of the potential energy for mass-asymmetric shape distortions on the fission path, after an idea of M. Itkis et al. [59]. The black curve shows the macroscopic potential that is minimum at symmetry, while the red curve includes the extra binding due to an assumed shell appearing at $N = 90$ in the heavy fragment.

Fig. 7. Schematic drawing of the potential energy as a function of a collective coordinate that is orthogonal to the fission direction at a fixed elongation. The two harmonic oscillator potentials with different depths and $\hbar\omega$ values represent the potential in two fission valleys for mass-asymmetric distortions that are related to different fission channels. The energies of the stationary states are indicated by the red horizontal lines. The overlapping of the two curves illustrates the possibility that the fission valleys are divided by a higher ridge due to some additional deformation degrees of freedom.

and the heavy fission fragment. Thus, these shells do not primarily depend on the fissioning system but on the number of neutrons and protons in the two fission fragments. However, these shells may be substantially different from the shell effects of the fragments in their ground state, because the nascent fragments in the fissioning di-nuclear system might be strongly deformed due to the interaction with the complementary fragment.

Figure 6 illustrates schematically how the potential in the mass-asymmetry degree of freedom is influenced by shell effects. Different minima appear that define different fission valleys. Due to the interplay of macrocopic and microscopic potential, the fission-fragment mass distribution may change substantially from one fissioning systeme to another, even though the shell effects on the fission path are essentially the same. The potential energy in the mass-asymmetric degree of freedom is shown as the sum of the macroscopic potential and one schematially assumed shell centered at $N = 90$. While the minimum of the macroscopic potential, which is at symmetry, is rather close to $N = 90$ in the heaviest systems, it moves away further in the lighter systems. Thus, the potential is minimum for asymmetric splits for the heavier system, favouring the population of the asymmetric fission channel, while the potential is minimum for symmetric splits for the lighter system, favouring the population of the symmetric fission channel. This behaviour explains qualitatively the transition from single-humped to double-humped mass distributions for fissioning systems around $A = 226$ depicted in fig. 4.

For a quantitative description, the motion in the mass-asymmetry degree of freedom may be represented by several weakly coupled quantum oscillators in thermal equi-
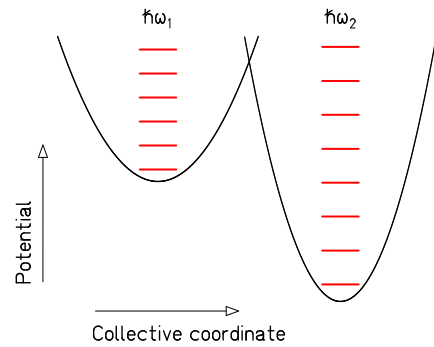
librium with a heat bath[2] of temperature T. The ratio of the yields Y_i of two fission channels corresponding to the population of two harmonic quantum oscillators depicted in fig. 7 is given by

$$Y_2/Y_1 = e^{-\Delta E/T} \cdot \frac{\hbar\omega_1}{\hbar\omega_2} \approx e^{-\Delta E/T}. \qquad (4)$$

ΔE is the potential-energy difference between the bottoms of the two quantum oscillators. The relation is strongly dominated by the exponential term.

The distribution of the collective coordinate in one fission channel is a Gaussian function with a variance σ^2 that is given by the well known equation:

$$\sigma^2 = \frac{\hbar\omega}{2C}\coth(\frac{\hbar\omega}{2T}). \qquad (5)$$

It is well known [63] that the statistical model, applied to the scission-point configuration, is unable of explaining the variances of the mass and energy distributions and their dependence on the compound-nucleus fissility. Studies of Adeev and Pashkevich [65] suggest that dynamical effects due to the influence of inertia and dissipation can be approximated by considering the properties of the system at an earlier time. That means that the statistical model may give reasonable results if it is applied to a configuration that depends on the typical time constant of the collective coordinate considered. The memory time is specific to the collective degree of freedom considered. It is relatively long for the mass-asymmetric distortions [66] and rather short for the charge-polarisation degree of

---

[2] According to Nörenberg [64], this heat bath comprises only the collective coordinates, because the coupling between collective and intrinsic motion is to weak to establish equilibrium between all degrees of freedom.

freedom [67–70]. Thus, the shape of the potential and the value of the respective collective temperature T that are decisive for the distribution of the respective observable are those that the system takes at the respective memory time before scission, which can be considered as a kind of freeze-out. This way, the parameters that are adjusted to the experimental distributions include dynamical effects.

Stochastic calculations [7] suggest that the fluctuations in mass asymmetry continue to evolve after the decision for a specific fission channel is already made. In the picture of coupled quantum oscillators, this suggests that the transfer of nucleons between different oscillators that represent the different fission channels is inhibited rather early, because the fission valleys may be divided by a high ridge due to some additional deformation degrees of freedom, while the width of the distribution in the respective quantum oscillator still increases on the way to scission. Thus, the two temperature values in equations (4) and (5) are separately determined by an adjustment to the characteristics of the yields and the widths of the fission channels, respectively.

It was possible to reproduce the measured mass distributions of the systems marked in fig. 4 by the contributions of four fission channels with a unique parameterisation: The symmetric fission channel corresponding to the macroscopic potential and three asymmetric fission channels linked to different fragment shells. These fission channels correspond to the super-long (SL), the standard 1 (S1), the standard 2 (S2) and the super-asymmetric (S3) fission channel in the Brosa terminology [28]. Their positions are determined by shells in the heavy fragment. In addition, the local enhancement of the standard 1 fission channel in plutonium isotopes is associated to a weaker shell in the light fragment that is complementary to the fragment in the standard 1 channel in the heavy fragment. Some shells in these light nuclei around $Z = 40$ seem to be responsible also for the double-humped distributions found for example in the fission of ^{201}Tl and ^{180}Hg. The same shapes and the same depths of the shells that form the asymmetric fission valleys were used for all systems. The positions of these shells were described with a global parameterisation. The shaded area in fig. 4 indicates the region where experimental data have been used to adjust the model parameters. Therefore, this area represents the domain of validity of our approach.

The observed system-dependent position of the asymmetric fission component that is dominated by the standard 2 fission channel is shown in fig. 8. The mean positions of the shell-stabilised heavy fragments of the different fission channels in thermal-neutron-induced fission are given by the following empirical relations:

For the S1 channel:

$$\bar{Z}_{S1} = 51.5 + 25 \cdot \left(\frac{Z_{CN}^{1.3}}{A_{CN}} - 1.5\right) \qquad (6)$$

For the S2 channel:

$$\bar{Z}_{S2} = 53.4 + 21.67 \cdot \left(\frac{Z_{CN}^{1.3}}{A_{CN}} - 1.5\right) \qquad (7)$$
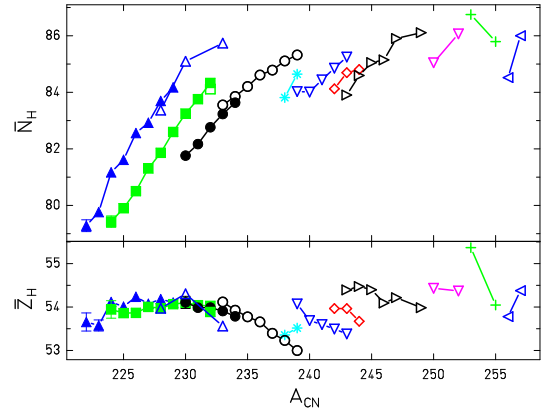

Fig. 8. Mean neutron and proton number of the heavy component in asymmetric fission in the actinide region before the emission of prompt neutrons. The values of $\overline{N_H}$ and $\overline{Z_H}$ that were not directly measured were deduced from measured mass or nuclear-charge distributions using the GEF model for the correction of charge polarisation and prompt-neutron emission. Open symbols denote results from conventional experiments, full symbols refer to an experiment with relativistic projectile fragments of ^{238}U [19]. Data points for the same Z_{CN} are connected. (See ref. [26], tables 8-10, for references of the underlying experimental data). The figure is taken from ref. [55]

For the S3 channel:

$$\bar{Z}_{S3} = 58.0 + 21.67 \cdot \left(\frac{Z_{CN}^{1.3}}{A_{CN}} - 1.5\right) \qquad (8)$$

The exact position of the shell around $Z = 42$ in the light fragment that enhances the yield of the S1 channel in fissioning nuclei around Pu is:

$$\bar{Z}_{light} = 42.15. \qquad (9)$$

The shell in the light fragment that enhances the yield of the S3 channel in fissioning nuclei around Cf has a slightly different position:

$$\bar{Z}_{light} = 39.7. \qquad (10)$$

Note that these values are the sum of the position of the fragment shell and the part of the neck that ends up in the respective fragment. Therefore, it is possible that these two values refer to the same shell, considering that the part of the neck that ends up in the light fragment may depend on the size of the heavy fragment.

The positions of the fission channels in fragment mass vary with increasing excitation energy. They are determined by searching for the mass-asymmetry degree of freedom that provides the highest level density at the given excitation energy in the respective fission valley.

The curvature of the macroscopic potential at the moment of freeze-out was taken from an analysis of Rusanov et al. [71] of the width of the symmetric component in measured fission-fragment distributions. The shape of the potential for mass-asymmetric distortions of this degree

of freedom is given by the sum of the macroscopic and the microscopic contribution. All these contributions are parameterised as parabolas $U = U_0 + C \cdot (Z - Z_0)^2$ in the vicinity of their minima, except for the S2 fission channel, where the potential has a more complex shape. The parameterisation as a function of Z was chosen by practical reasons, because the position of the fission channels is almost constant in Z, see fig. 8. The mass number A is then given by the mean charge polarisation. The values of the stiffness coefficients C used in the GEF code are listed in table 1.

Table 1. Stiffness coefficients of the different contributions to the potential for mass-asymmetric distortions. The stiffness of the macroscopic potential depends on the system. It is taken from ref. [71].

macroscopic	S1	S3	$Z \approx 42$
systematics [71]	0.30 MeV	0.076 MeV	0.28 MeV

The shell that forms the S2 channel is parameterised as a rectangular distribution in particle number with a width of $\Delta Z = 5.6$. The borders are smoothed by a parabolic shape with $C = 0.174$ MeV at the lower side and with $C = 0.095$ MeV at the upper side. This is technically performed by convoluting the rectangular distribution with two Gaussian distributions with different width around the two borders of the rectangle. This kind of shape is consistent with the general feature of deformed shells obtained from shell-model calculations, [72–76], which show extended valleys in the 2-dimensional plane of particle number and deformation that start at a specific particle number at small deformation and extend to a larger particle number at large deformation with a rather constant shell effect over the whole range.

The strengths of the fragment shells are listed in table 2. The strength of the shell behind the S1 fission channel varies as a function of neutron excess, because it is created by both, the $Z = 50$ and the $N = 82$ shells. Thus, its strength decreases if the N/Z ratio of the fissioning system deviates from the one of the doubly magic ^{132}Sn.

$$\delta U_{eff} = -1.8 \text{ MeV} \cdot (1 - 4.5 \cdot |82/50 - N_{CN}/Z_{CN}|) \quad (11)$$

The maximum value of the effective shell strength δU_{eff} is the sum of the shell strength $\delta U = -4.6$ MeV and the expense $\Delta U_{mac} = 2.8$ MeV to be paid to the macroscopic potential due to the spherical shape that is energetically unfavourable at scission.

The population of states in the different fission valleys behind the outer fission barrier that rule the yields of the fission channels according to eq. (4) is determined by the effective temperature of the density of nuclear states, that is the inverse logarithmic slope of the level density according to the modified composite level-density formula of ref. [77]. In the superfluid regime, the values in the actinide region are around 0.4 MeV [78]. As discussed above, this

Table 2. Strengths of the fragments shells near the outer fission barrier.

S2	S3	$Z \approx 42$
-4.0 MeV	-6.0 MeV	-1.3 MeV

is expected if the population of the fission channels is decided at or close to the outer saddle, where all degrees of freedom are in statistical equilibrium [57].

For excitation energies below the height of the outer barrier, e.g. for spontaneous fission, eq. (4) must be extended in order to account for tunneling. In this case, the yield of a specific fission channel i is calculated with the following equation:

$$Y_i = \frac{e^{E_{sad}^{*,i}/T}}{1 + e^{(-E_{sad}^{*,i}/(T \cdot T_{tun}^i/(T - T_{tun}^i)))}} \quad (12)$$

Y_i is not normalised. This is not necessary, because only relative yields are needed.

The temperature parameter T_{tun}^i describes the part of the transmission coefficient through the outer fission barrier that is sensitive to the specific properties of the corresponding fission channel. The values of the temperature parameters for the different fission channels are given in table 3. Note that the transmission through the first barrier and part of the transmission through the second barrier is common for all fission channels. Only the last part of the trajectory towards the exit point in the respective fission valley is specific to the fission channel. Because the common part cancels when calculating relative yields, it is not included in eq. (12).

Table 3. Temperature parameter T_{tun}^i for the calculation of the effective transmission coefficients through the outer fission barrier. The values are given for the different fission channels.

SL	S1	S2	S3
0.31 MeV	0.342 MeV	0.31 MeV	0.31 MeV

The temperature parameter that determines the widths of the distributions of the different fission channels in mass according to eq. (5) is parameterised in the GEF code by the relation

$$T = 0.034 \cdot E_{sad}^* + 0.04 \cdot \Delta E_{sad-sci}. \quad (13)$$

E_{sad}^* is the excitation energy of the fissioning system above the respective outer saddle, $\Delta E_{sad-sci}$ is the potential energy gain from saddle to scission [79]. E_{sad}^* becomes negative for excitation energies below the height of the outer barrier, e.g. for spontaneous fission. The value of $\hbar\omega/2$ for the S1 fission channel that determines the minimum width due to the zero-point motion is 0.48 MeV. The distributions of the other fission channels are assumed to be well described by the classical limit.
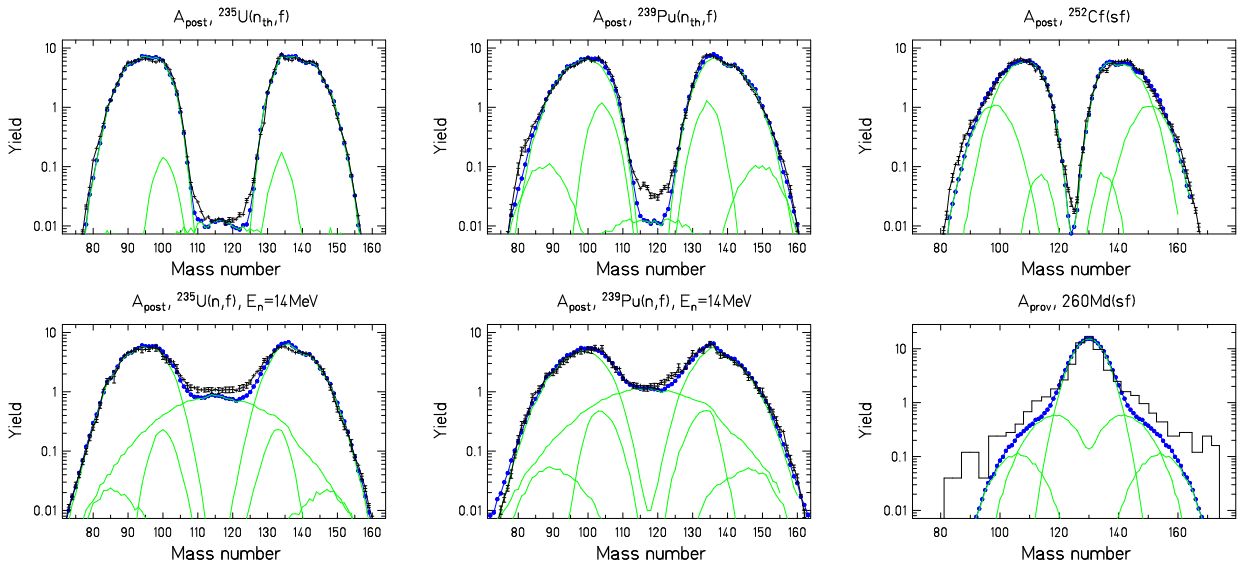
Fig. 9. Evaluated and measured mass distributions (black symbols) of fission fragments in comparison with the result of the GEF model (blue symbols). The mass distribution after prompt-neutron emission are taken from the evaluation of ref. [80]. The provisional masses from spontaneous fission of ^{260}Md were directly deduced from the ratio of the fragment energies without applying a correction for prompt-neutron emission. They are taken from ref. [62]. The green lines show the calculated contributions from the different fission channels. The figure is taken in parts from ref. [26]

The width of the charge polarisation is completely determined by the zero-point motion [69].

More details of the parameterisation used in the GEF model can be found in ref. [26].

Figure 9 demonstrates the good reproduction of the measured, respectively evaluated mass distributions of several systems. The narrow symmetric peak appearing in the system ^{260}Md(sf) is produced by the overlap of the shell near ^{132}Sn in both fragments. Note that the distributions from 14-MeV-induced fission are not directly parameterised but determined as the sum of the contributions from the different fission chances. Competition between pre-equilibrium particle emisssion, neutron evaporation, gamma emission, and fission is taken into account by a statistical code that forms part of the GEF model. See ref. [26] for details.

4 Energetics of the fission process

In low-energy fission, the available energy, consisting of the Q value of the reaction plus the initial excitation energy of the fissioning nucleus, ends up either in the total kinetic energy (TKE) or the total excitation energy (TXE) of the fragments. Moreover, the TXE is divided between the two fission fragments. The main contributions to the excitation energies of the final fragments are the initial excitation energy of the fissioning system minus the outer fission barrier, the dissipated energy between outer fission barrier and scission, and the gain of binding energy when the fragments snap to their ground-state shape after scission.

Theoretical investigations of the gradual transition on the way from the fission barrier to the scission configuration, from a mono-nuclear to a di-nuclear system show that the properties of the individual fission fragments are already well established not far behind the outer saddle, not only concerning shell effects [22] as discussed in sect. 3, but also with respect to pairing correlations [81] and the congruence energy [82]. If the dynamic evolution of the system between the fission barrier and scission is slow enough, the system formed by the two nuclei in contact then evolves to a state of statistical equilibrium, the macro-state of maximum entropy, where all the available micro-states have equal probability [83]. This implies that the intrinsic excitation energy will be distributed among the two nascent fragments according to the probability distribution of the available microstates which is given by the total nuclear level density[3].

Thus, the distribution of excitation energy E_1 of one fragment is given by the statistical weight of the states with a certain division of excitation energy between the fragments:

$$\frac{dN}{dE_1} \propto \rho_1(E_1) \cdot \rho_2(E_{tot} - E_1) \qquad (14)$$

Note that ρ_1 and ρ_2 are the level densities of the fragments in their shape between saddle and scission, not in their ground-state shape. The remaining energy $E_{tot} - E_1$ is taken by the other fragment.

---

[3] The degeneracy of magnetic sub-states is not considered, because it contributes very little to the variation of the density of states as a function of excitation energy.
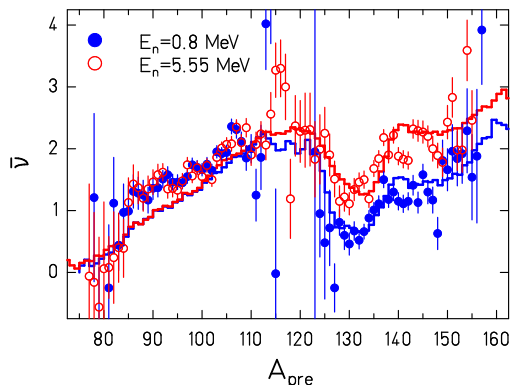
Fig. 10. Measured prompt-neutron multiplicity in ^{237}Np(n,f) for $E_n = 0.8$ MeV and 5.55 MeV [95] as a function of the pre-neutron fragment mass (data points) in comparison with the result of the GEF model (histograms). The figure is taken from ref. [26].

In the regime of pairing correlations, the level density was found to grow almost exponentially with increasing excitation energy [84–91]. This can be understood by the phase transition from superfluidity to a Fermi gas, which is characterised by a strong increase of the effective degrees of freedom by pair breaking, leading to an essentially constant nuclear temperature [92]. In this energy regime, energy sorting will take place, and the light fragment will transfer essentially all its excitation energy to the heavy one [93,94]. At higher energies, in the independent-particle regime where pairing correlations die out, there is a gradual transition to a division closer to the ratio of the fragment masses according to the validity of the Fermi-gas level density.

The phenomenon of energy sorting explains in a straightforward and natural way the finding of ref. [95] demonstrated in fig. 10 that the additional energy introduced in neutron-induced fission of ^{237}Np raises the neutron multiplicities in the heavy fragment, only. A similar result was reported for the system ^{235}U(n,f) [96], but data of this kind for other systems with good quality are scarce.

The saw-tooth behaviour of the prompt-neutron yield as a function of fragment mass, seen in fig. 10 and found in low-energy fission of all systems in the actinide region, has been attributed to the fragment shells at large fragment deformation in the scission-point model of ref. [74], in particular to the correlation between nucleon number and optimum deformation obtained from the shell model, that was mentioned before.

In the GEF model, the deformation of the fragments at scission is approximated by a second-order spheroid with a tip distance of 1 fm. The deformation parameter β of the heavy fragment of the S2 fission channel is parameterised as a linear function of the atomic number Z_{heavy}:

$$\beta_{heavy} = 0.0275(Z_{heavy} - 48.0). \tag{15}$$

The deformation of the light fragment of the S1 and the S2 fission channels is given by:

$$\beta_{light} = 0.0325(Z_{light} - 24.5). \tag{16}$$

We assume that this is due to a shell, roughly in the region $28 < Z < 50$. It was not possible to deduce the strength of this shell from the fission observables, but it is certainly weaker than the shells in the heavy fragment, because this shell in the light fragment does not influence the positions of the S1, S2 and S3 fission channels.

Deviating from this behaviour, the nascent heavy fragment of the S1 channel is assumed to be spherical.

The deformation parameters of the nascent fragments of the super-long (symmetric) fission channel were determined by minimising the macroscopic potential energy (binding energies of the fragments plus Coulomb interaction potential) at the scission configuration.

The deformation values of the fragments belonging to the S3 fission channel are not well defined, because the S3 channel is covered to a great part by much stronger fission channels in all fissioning systems. Best agreement with the data is obtained when the deformation of the heavy fragment is given by

$$\beta_{heavy} = 0.0275(Z_{heavy} - 48.0) + 0.2 \tag{17}$$

and the deformation of the light fragment is formulated as

$$\beta_{light} = 0.0325(Z_{light} - 24.5) - 0.1. \tag{18}$$

In the far left tails of the distributions, where the equations (15) to (18) eventually give negative values, spherical shape ($\beta = 0$) is assumed.

For fissioning nuclei around Pu, where the shell around ^{132}Sn in the heavy fragment meets the shell near $Z = 42$ in the light fragment, the deformation of the light fragment deviates from the above description. The TKE values and the prompt-neutron yields indicate that the shell near $Z = 42$ favours less deformed fragments at scission. This deviation is parameterised accordingly in the GEF code.

Since the fragment deformation, except in the SL channel, is strongly influenced by shell effects, there should be a universal behaviour of the prompt-neutron yield as a function of the fragment size for the asymmetric fission channels that are dominant in the actinide region. Figure 11 demonstrates that a good reproduction of the prompt-neutron yield for spontaneous fission can be obtained with this approach. For most systems, the prompt-neutron yield shows the systematic increase with Z and A of the fissioning nucleus that is found in all systems, where the S2 fission channel dominates. However in the neutron-rich plutonium isotopes the prompt-neutron yield deviates to lower values due to the stronger yield of the more compact S1 fission channel with an almost spherical heavy fragment at scission. This reduction is even stronger in fermium isotopes approaching ^{258}Fm, where the two fragments are formed in a very compact configuration in almost spherical shape.
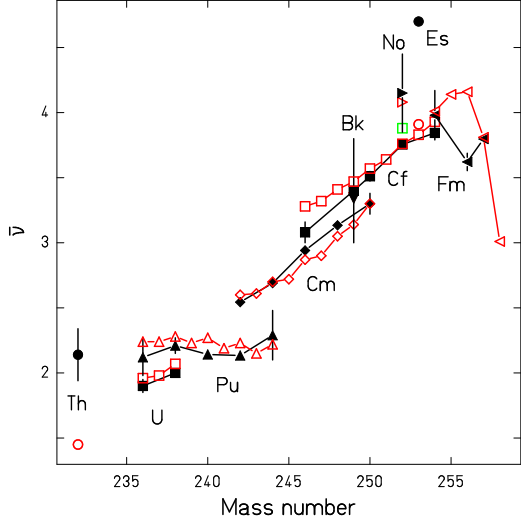
Fig. 11. Measured mean prompt-neutron multiplicities for spontaneous fission (black full symbols) as a function of the mass number of the fissioning nucleus [97] in comparison with the result of the GEF model (red open symbols). Experimental error bars are not shown when they are smaller than the symbols. The value for ^{253}Es is reported without an experimental uncertainty. The figure is taken from ref. [26].
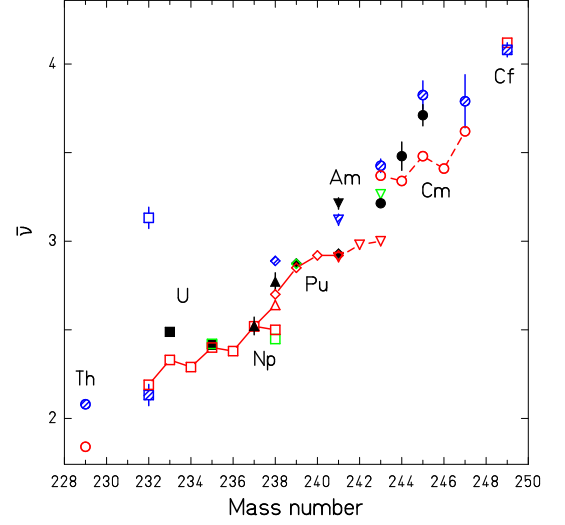

Fig. 12. Measured mean prompt-neutron multiplicities for thermal-neutron induced fission as a function of the mass number of the target nucleus [98] (black full symbols), [97] (blue shaded symbols), and [99] (green open symbols) in comparison with the result of the GEF model (red open symbols). We assumed that the value 3.132 for ^{232}U given in [97] (blue open symbol) is wrong due to a misprint. The tentatively corrected value (2.132) is marked by a blue shaded symbol. Experimental error bars are not shown when they are smaller than the symbols. The figure is taken from ref. [26].

The prompt-neutron yields from thermal-neutron induced fission, shown in fig. 12, are also rather well reproduced. However, the deviations are larger. It is not clear, whether this is a deficiency of the model. The discrepancies found between the results of different experiments may also indicate larger experimental uncertainties due to the difficulties in the suppression of background from scattered neutrons.

Not only the prompt-neutron yield is a signature of the energetics of the fission process. Also the odd-even effect in the fragment Z distribution gives very interesting information [100]. The quantitative calculation of the odd-even effect is based on the assumption that the distribution of excited states in the two fragments at scission is in statistical equilibrium. This means that each state of the fissioning system is populated with the same probability.

For an even-even fissioning nucleus, the number of configurations with Z_1 even at fixed total reduced energy U_{tot} is given by:

$$N^{ee}_{Z_1=e}(Z_1) = \int_{-2\Delta_1}^{U_{tot}+2\Delta_2} \rho_1(U_1)_{(ee)}\rho_2(U_{tot}-U_1)_{(ee)}dU_1+$$

(19)

$$\int_{-\Delta_1}^{U_{tot}+\Delta_2} \rho_1(U_1)_{(eo)}\rho_2(U_{tot}-U_1)_{(eo)}dU_1$$

where $\rho_i(U_i)_{(ee)}$ and $\rho_i(U_i)_{(eo)}$ are the level densities of representative even-even and odd-even fragments, respectively, with mass close to A_1 or A_2. The reduced energy U is shifted with respect to the energy E above the nuclear ground state: $U = E - n\Delta$, $n = 0, 1, 2$ for odd-odd, odd-mass, and even-even fragments, respectively. This ensures the use of a common energy scale in the frame of the fissioning system with respect to odd-even fluctuations, independently of the number of neutrons and protons in the fragments, which is a basic requirement for the application of statistical mechanics.

The number of configurations with Z_1 odd for an even-even fissioning nucleus is:

$$N^{ee}_{Z_1=o}(Z_1) = \int_{-\Delta_1}^{U_{tot}-\Delta_2} \rho_1(U_1)_{(oe)}\rho_2(U_{tot}-U_1)_{(oe)}dU_1+$$

(20)

$$\int_{0}^{U_{tot}} \rho_1(U_1)_{(oo)}\rho_2(U_{tot}-U_1)_{(oo)}dU_1$$

where $\rho_i(U_i)_{(oe)}$ and $\rho_i(U_i)_{(oo)}$ are the level densities of representative odd-even and odd-odd nuclei, respectively, with mass close to A_1 or A_2. The yield for even-Z_1 nuclei is $Y^{ee}_{Z_1=e}(Z_1) = N^{ee}_{Z_1=e}(Z_1)/N^{ee}_{tot}/(Z_1)$ with $N^{ee}_{tot}(Z_1) =$
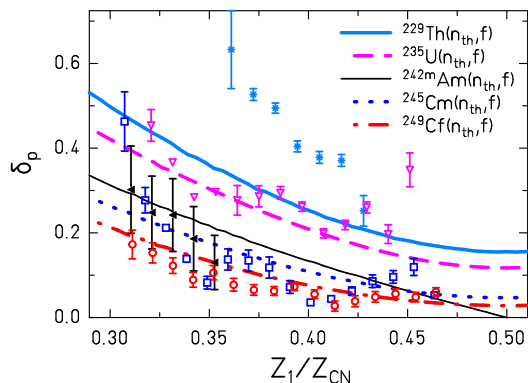
Fig. 13. Local odd-even effect δ_p as a function of asymmetry. The symbols represent experimental data from the compilation of ref. [21] and denote the target nuclei: ^{229}Th (stars), ^{235}U (open triangles), ^{242}Am (full triangles), ^{245}Cm (open squares), ^{249}Cf (open circles). The lines correspond to the results of the GEF model. The figure is taken from ref. [100].

$N_{Z_1=e}^{ee}(Z_1) + N_{Z_1=o}^{ee}(Z_1)$. Similar equations hold for odd-even, even-odd and odd-odd fissioning systems. The total available reduced intrinsic excitation energy U_{tot} is assumed to be a fraction of the potential-energy difference from saddle to scission plus the initial excitation energy above the barrier. Thus, it increases with the Coulomb parameter $Z^2/A^{1/3}$ of the fissioning nucleus.

This approach reproduces the observed salient features of the odd-even effect [21]: (i) The mean odd-even effect $(\Sigma Y_{Z=e} - \Sigma Y_{Z=o}) / (\Sigma Y_{Z=e} + \Sigma Y_{Z=o})$ decreases with the Coulomb parameter and with increasing intitial excitation energy. (ii) The local odd-even effect $\delta_p(Z+3/2) = 1/8(-1)^{Z+1}(\ln Y(Z+3) - \ln Y(Z) - 3[\ln Y(Z+2) - \ln Y(Z+1)])$ increases towards mass asymmetry. (iii) The local odd-even effect for odd-Z fissioning nuclei is zero at mass symmetry and approaches the value of even-Z nuclei for large mass asymmetry. As shown in fig. 13, the quantitative reproduction is satisfactory, except for the system ^{229}Th(n$_{th}$,f). The disagreement found for this system may be caused by the neglect of fluctuations in the dissipated energy. In fact, for a great part of the fission events the available energy may be so low that they reach the scission point in a completely paired configuration due to the threshold character of the first quasi-particle excitation.

As discussed in [100], the odd-even effect in fission-fragment Z distribution is a sign of an extreme energy-sorting process. It documents the entropy-driven enhanced production of a cold even-even fully paired light fragment in its ground state.

5 Discussion

The study of the fission barriers demonstrates clearly that it is possible to construct a description on the basis of the

topographic theorem that is able to reproduce the empirical barrier heights essentially within the error bars. This unprecedented accuracy can presently not be attained by a microscopic theory. Also predictions towards more or less neutron-rich isotopes can certainly be made rather reliably to a certain extent, as long as empirical atomic-mass values are available. An essential feature of this approach is that theory only provides the macroscopic energies at the fission barrier (E_f^{mac}) and in the nuclear ground-state (E_{gs}^{mac}), while the influence of shell effects on the fission barrier is provided by the measured nuclear energy E_{gs}^{exp} in the ground state. This study also revealed very clearly that the odd-even fluctuations in the fission-barrier height exceed those in the ground-state masses appreciably, indicating a larger pairing strength at the barrier. However, it should be stressed that the reproduction of the isotopic trend by use of the topographic theorem depends on the quality of the model that is used to calculate the macroscopic mass at the fission barrier. Different models may give strongly diverging results. This is clearly demonstrated in refs. [50,101]. The droplet model [102], for example, was found to predict an isotopic trend that deviates strongly from the trend of the empirical data [101].

However, there remain questions, that claim for a careful study on a microscopic level. These studies could clarify, whether the increased odd-even fluctuations at the barrier are caused by a deformation dependence of the pairing strength that would indicate a contribution from surface pairing. Another explanation would be a reduced pairing-gap parameter in the ground state of the heavier actinides due to a small single-particle level density caused by their large negative ground-state shell effect. A larger single-particle level density at the barrier, that is probably characterized by a positive shell effect (less binding), could possibly explain that the gap parameter Δ_f is appreciably larger than the average gap parameter deduced from the odd-even staggering of the ground-state masses. The fact that the odd-even fluctuations of the macroscopic-microscopic model of ref. [35], which takes the influence of the single-particle level density at the Fermi surface into account, are too weak, suggests the presence of a strong contribution from surface pairing.

Further studies could also find the reason for the need of the Z-dependent shift ΔB_f in eq. (2). The rather systematic behaviour of the shift suggests that it is a macroscopic effect. It could be a deficiency of the predictions of the Thomas-Fermi model of ref. [23,51] for the Z dependence of the macroscopic ground-state or the saddle-point masses. The kink at $Z = 90$ could be an indication for a violation of the topographic theorem. It is striking that for $Z = 90$ the location (in terms of elongation of the system) of the macroscopic barrier coincides with the location of the second minimum. Thus, the contribution of the macroscopic potential to the fission-barrier height is minimum around $Z = 90$ and systematically increases towards both lighter and heavier nuclei, because the maximum of the macroscopic potential approaches the location of the inner or the outer barrier for heavier or lighter nuclei, respectively. Another problem to be tackled by microscopic

models would be to explore to which extent the macroscopic description of the Thomas-Fermi fission barriers of ref. [23] can reliably be extrapolated towards very exotic nuclei, *e.g.* towards the astrophysical r-process path. We would like to stress that saddle-point masses seem to be only little affected by shell effects. Thus they are well suited to benchmark macroscopic aspects of microscopic models. This is particularly important for very exotic nuclei, because the precision of macroscopic trends becomes increasingly important for predicting properties of nuclei at larger distances from well studied nuclei.

The description of the properties of the fission fragments by the GEF model appears to be estonishingly simple and schematic. But the good reproduction of the experimental data indicates that the essential features of the fission process are well represented, and the approximations are not crucial. The most powerful asset of the GEF model is the separability principle of the macroscopic properties of the mononucleus and the microscopic properties of the nascent fragments. Like the description of the fission barriers with the topographic theorem, it is based on the macroscopic-microscopic approach. The separability principle reduces the complexity of an individual very specific potential-energy surface for each fissioning system calculated by microscopic models to the superposition of universal shells in only four systems: the proton and neutron subsystems of the two nascent fragments as a function of particle number and deformation. In addition to the good agreement with measured data, the simplicity of the GEF model reveals that the underlying features of the fission process change gradually and systematically as a function of the fissioning system and its excitation energy, even if uprupt changes appear in the observables.

Nevertheless, the situation is not fully satisfactory. For example, the fragment shells that are behind the fission channels could not precisely be identified. Instead, the GEF model has to directly use empirical information. In particular, the rather constant position of the heavy asymmetric fragment component in atomic number for fissioning nuclei in the actinide region, which seems to be incompatible with the expected dominant role of neutron shells for asymmetric fission [74], is not understood. Moreover, some of the model parameters cannot be determined unambiguously by the experimental data. For example, the variance of the distribution of a fission channel is given by the inverse of the ratio of the curvature C of the potential in a fission valley for mass-asysmmetric distortions and the corresponding collective temperature T in the classical limit, see eq. (5). Thus, the value of C/T is well determined, but the individual values of C and T are not well confined. The solution of these problems is probably only possible with the help of microscopic models. However, this does not seem to be an easy task, regarding the large discrepancies between fission barriers obtained from microscopic models and empirical values. While nuclear ground-state masses can be obtained with an uncertainty of about 500 keV by the most reliable microscopic models, the potential energy at large deformation seems to be subject to an uncertainty around 1 MeV. Being off in the calculation of the depth of the potential in a fission valley by this amount changes the corresponding fragment yield by more than an order of magnitude in low-energy fission according to eq. (4). This makes it rather difficult to draw definite conclusions.

A general lesson that can be drawn from the present work is that certain aspects of the macroscopic-microscopic approach should not be considered as obsolete, as one may be tempted by the considerable progress in microscopic modelling. For example, self-consistent microscopic calculations of the macroscopic nuclear properties with the Thomas-Fermi model or similar approaches that average over nuclear-structure effects could be very helpful in establishing a reliable basis for extrapolating fission barriers towards nuclei further away from beta stability. Also the separability principle that suggests the universal character of the shell structure on the fission path by the strong influence of fragment shells demonstrates the benefit of the distinction of macroscopic and microscopic nuclear properties for a general high-precision description of fission-fragment properties.

6 Conclusion

It has been shown that the assumption that the macroscopic potential energy is a property of the fissioning nucleus, whereas shell effects are essentially defined by the fragments, as well as the assumption of statistical equilibrium for a system made of two fragments in thermal contact can explain many complex observations, revealing a significant regularity in the fission process that is not apparent when directly watching the observables. These regularities are often also not accessible to microscopic models. When combining these regularities with the available empirical information, it was possible to develop a model description of fission observables with an unprecedented precision. We expect a good predictive power in a broad region extending from Po to Sg isotopes. Our general approach can be extended to other regions if there exists sufficient experimental information to adjust the model parameters. Moreover, explanations were found for several observed features that were not understood for decades. However, a few observed features could only be described in a purely phenomenological way. These ask for an explanation on the microscopic level. It may be concluded that global approaches contribute to better understand the physics of the nuclear-fission process and, moreover, a combination of global and microscopic methods could be a way to overcome the difficulties in meeting the increasing need of nuclear data with the required precision for the existing and future emerging nuclear applications.

References

1. P. Möller, D. G. Madland, A. J. Sierk, and A. Iwamoto, Nature **409**, 785 (2001).
2. T. Asano, T. Wada, M. Ohta, T. Ichikawa, S. Yamaji, and H. Nakahara, J. Nucl. Radioch. Sc. **5**, 1 (2004).
3. T. Asano, T. Wada, M. Ohta, S. Yamaji, and H. Nakahara, J. Nucl. Radioch. Sc. **7**, 7 (2006).
4. J. Randrup, P. Möller, and A. J. Sierk, Phys. Rev. C **84**, 034613 (2011).
5. P. Möller, J. Randrup, and A. J. Sierk, Phys. Rev. C **85**, 024306 (2012).
6. Y. Aritomo and S. Chiba, Phys. Rev. C **88**, 044614 (2013).
7. Y. Aritomo, S. Chiba, and F. Ivanyuk, Phys. Rev. C **90**, 054609 (2014).
8. H. Goutte, J. F. Berger, P. Casoli, and D. Gogny, Phys. Rev. C **71**, 024316 (2005).
9. C. Simenel and A. S. Umar, Phys. Rev. C **89**, 031601 (2014).
10. M. Mirea, L. Tassangot, C. Stephan, and C. O. Bacri, Nucl. Phys. A **735**, 21 (2004).
11. R. Bernard, H. Goutte, D. Gogny, and W. Younes, Phys. Rev. C **84**, 044308 (2011).
12. H. Goutte, contribution to this conference.
13. *Compilation and evaluation of fission yield nuclear data*, TECDOC-1168, IAEA, Vienna, 2000.
14. *Fission-product-yield data for the transmutation of minor actinide nuclear waste*, STI/PUB/1286, IAEA, Vienna, 2008.
15. R. Vogt and J. Randrup , Phys. Rev. C **84**, 044621 (2011).
16. R. Vogt, J. Randrup, D. A. Brown, M. A. Descalle, and W. E. Ormand , Phys. Rev. C **85**, 024608 (2012).
17. J. P. Lestone , Nucl. Data Sheets **112**, 3120 (2011).
18. P. Talou, T. Kawano, I. Stetcu, R. Vogt, and J. Randrup, Nucl. Data Sheets **118**, 227 (2014).
19. K.-H. Schmidt, S. Steinhäuser, C. Böckstiegel, A. Grewe, A. Heinz, A. R. Junghans, J. Benlliure, H.-G. Clerc, M. de Jong, J. Müller, M. Pfützner, and B. Voss, Nucl. Phys. A **665**, 221 (2000).
20. C. Böckstiegel, S. Steinhäuser, K.-H. Schmidt, H.-G. Clerc, A. Grewe, A. Heinz, M. de Jong, A. R. Junghans, J. Müller, and B. Voss, Nucl. Phys. A **802**, 12 (2008).
21. M. Caamano, F. Rejmund and K.-H. Schmidt, J. Phys. G: Nucl. Part. Phys. **38**, 035101 (2011).
22. U. Mosel and H. W. Schmitt, Phys. Rev. C **4**, 2185 (1971).
23. W. D. Myers and W. J. Swiatecki, Nucl. Phys. A **601**, 141 (1996).
24. K.-H. Schmidt, A. Kelic, and M. V. Ricciardi, Europh. Lett. **83**, 32001 (2008).
25. K.-H. Schmidt and B. Jurado, Phys. Rev. Lett. **104**, 21250 (2010).
26. K.-H. Schmidt, B. Jurado, and Ch. Amouroux, *General description of fission observables*, JEFF Report 24, Data Bank of the Nuclear Energy Agency of the OECD, 2014
27. V. V. Pashkevich, Nucl. Phys. A **169**, 175 (1971).
28. U. Brosa, S. Grossmann, and A. Mueller, Phys. Rep. **197**, 167 (1990).
29. J. Katakura, *A systematics of fission product mass yields with 5 Gaussian function*, JAERI Research 2003-004 (2003), Japan Atomic Energy Research Institute (JAERI).
30. D. M. Gorodisskiy, S. I. Mulgin, V. N. Okilovich, A. Ya. Rusanov, and S. V. Zhdanov, Phys. Lett. B **548**, 45 (2002).
31. U. Brosa, H.-H. Knitter, Tie-shuan Fan, Ju-min Hu, and Shang-lian Bao, Phys. Rev. C **59**, 767 (1999).
32. M. C. Dujvestijn, A. J. Koning, and F.-J. Hambsch, Phys. Rev. C **64**, 014607 (2001).
33. G. Royer and C. Bonilla, J. Radioanalytical Nuclear Chemistry **272**, 237 (2007).
34. A. Dobrowolski, K. Pomorski, and J. Bartel, Phys. Rev. C **75**, 024613 (2007).
35. P. Möller, A. J. Sierk, T. Ichikawa, A. Iwamoto, R. Bengtsson, H. Uhrenholt, and S. Aberg, Phys. Rev. C **79**, 064304 (2009).
36. M. Kowal, P. Jachimowicz, and A. Sobiczewski, Phys. Rev. C **82**, 014303 (2010).
37. M. Mirea and L. Tassan-Got, Centr. Eur. J. Phys. **9**, 116 (2011).
38. P. Jachimowicz, M. Kowal, and J. Skalski, Phys. Rev. C **85**, 034305 (2012).
39. M. Kowal and J. Skalski, Phys. Rev. C **85**, 061302 (2012).
40. H. Abusara, A. V. Afanasjev, and P. Ring, Phys. Rev. C **85**, 024314 (2012).
41. Bing-Nan Lu, En-Guang Zhao, and Shan-Gui Zhou, Phys. Rev. C **85**, 011301 (2012).
42. J.-P. Delaroche, M. Girod, H. Goutte, and J. Libert, Nucl. Phys. A **771**, 103 (2006).
43. S. Goriely, M. Samyn, and J. M. Pearson, Phys. Rev. C **75**, 064312 (2007).
44. F. Minato and K. Hagino, Phys. Rev. C **77**, 044308 (2008).
45. S. Goriely, S. Hilaire, A. J. Koning, M. Sin, and R. Capote, Phys. Rev. C **79**, 024612 (2009).
46. S. Goriely, N. Chamel, and J. M. Pearson, Phys. Rev. C **88**, 061302 (2013).
47. A. Sobiczewski and Y. A. Litvinov, Phys. Rev. C **89**, 024311 (2014).
48. F. A. Ivanyuk and K. Pomorski, Phys. Rev. C **79**, 054327 (2009).
49. A. V. Karpov, A. Kelic, and K.-H. Schmidt, J. Phys. G: Nucl. Part. Phys. **35**, 035104 (2008).
50. A. Kelic and K.-H. Schmidt, Phys. Lett. B **634**, 362 (2006).
51. W. D. Myers and W. J. Swiatecki, Phys. Rev. C **60**, 014606 (1999).
52. S. Bjoernholm and J. E. Lynn, Rev. Mod. Phys. **52**, 725 (1980).
53. M. G. Itkis, N. A. Kondrat'ev, S. I. Mul'gin, V. N. Okolovich, A. Ya. Rusanov, and G. N. Smirenkin, Sov. J. Nucl. Phys. **52**, 601 (1990).
54. A. N. Andreyev, J. Elseviers, M. Huyse, P. Van Duppen, S. Antalic, A. Barzakh, N. Bree, T. E. Cocolios, V. F. Comas, J. Diriken, D. Fedorov, V. Fedosseev, S.

Franchoo, J. A. Heredia, O. Ivanov, U. Koester, B. A. Marsh, K. Nishio, R. D. Page, N. Patronis, M. Seliverstov, I. Tsekhanovich, P. Van den Bergh, J. Van De Walle, M. Venhart, S. Vermote, M. Veselsky, C. Wagemans, T. Ichikawa, A. Iwamoto, P. Moeller, and A. J. Sierk, Phys. Rev. Lett. **105**, 252502 (2010).

55. K.-H. Schmidt and B. Jurado, EPJ Web of Conferences **62**, 06001 (2013).

56. S. I. Mulgin, K.-H. Schmidt, A. Grewe, and S. V. Zhdanov, Nucl. Phys. A **640**, 375 (1998).

57. E. Wigner, Trans. Faraday Sot. **34**, part 1, 29 (1938).

58. U. Mosel, H. W. Schmitt Nucl. Phys. A **165** (1971) 73

59. M. G. Itkis, V. N. Okolovich, A. Ya. Rusanov, and G. N. Smirenkin, Z. Phys. A **320**, 433 (1985).

60. F. Vives, F.-J. Hambsch, H. Bax, and S. Oberstedt, Nucl. Phys. A **662**, 63 (2000).

61. F.-J. Hambsch and S. Oberstedt, Nucl. Phys. A **617**, 347 (1997).

62. E. K. Hulet, J. F. Wild, R. J. Dougan, R. W. Lougheed, J. H. Landrum, A. D. Dougan, P. A. Baisden, C. M. Henderson, and R. J. Dupzyk, Phys. Rev. C **40**, 770 (1989).

63. Yu. Ts. Oganessian and Yu. A. Lazarev, *Heavy ions and nuclear fission*, in Treatise on Heavy Ion Science, Vol. 4, ed. D. A. Bromley, Plenum Press, New York, 1985, p. 1.

64. W. Nörenberg, *Unified theory of low-energy fission and fission models*, Proc. Symp. Phys. Chem. Fission, Rochester 1973, IAEA Vienna (1974), vol. 1, p. 547.

65. G. D. Adeev and V. V. Pashkevich, Nucl. Phys. A **502**, 405c (1989).

66. A. V. Karpov, P. N. Nadtochy, D. V. Vanin, and G. D. Adeev, Phys. Rev. C **63**, 054610 (2001).

67. H. Nifenecker, J. Physique Lett. **41**, 47 (1980).

68. M. Asghar, Z. Phys. A **296**, 79 (1980).

69. W. D. Myers, G. Manzouranis, and J. Randrup, Phys. Lett. B **98**, 1 (1981).

70. A. V. Karpov and G. D. Adeev, Eur. Phys. J. A **14**, 169 (2002).

71. A. Ya. Rusanov, M. G. Itkis, and V. N. Oklovich, Phys. At. Nucl. **60**, 683 (1997).

72. V. M. Strutinsky, Nucl. Phys. A **122**, 1 (1968).

73. M. Brack, J. Damgaard, A. S. Jensen, H. C. Pauli, V. M. Strutinsky, and C. Y. Wong, Rev. Mod. Phys. **44**, 320 (1972).

74. B. D. Wilkins, E. P. Steinberg, and R. R. Chasman, Phys. Rev. C **14**, 1832 (1976).

75. V. M. Strutinsky, A. G. Magner, S. R. Ofengenden, and T. Doessing, Z. Phys. A **283**, 269 (1977).

76. I. Ragnarsson, R. K. Sheline, Phys. Scr. **29**, 385 (1984).

77. K.-H. Schmidt and B. Jurado, Phys. Rev. C (**86**), 044322 (2012).

78. T. von Egidy, D. Bucurescu, Phys. Rev. C **80**, (2009) 054310.

79. M. Asghar and R. W. Hasse, J. Phys. Colloques **45** (1984) C6-455.

80. T. R. England and B. F. Rider, *Evaluation and compilation of fission product yields*, ENDF-349, LA-UR-94-3106, Los Alamos National Laboratory (1994); Available from http://t2.lanl.gov/publications/yields/apxA.txt .

81. H. J. Krappe, Int. J. Mod. Phys. E **16**, 396 (2007).

82. W. D. Myers and W. J. Swiatecki, Nucl. Phys. A **612**, 249 (1997).

83. D. H. Gross, Entropy **6**, 158 (2004) / Special Issue Quantum Limits to the Second Law of Thermodynamics.

84. M. Guttormsen, R. Chankova, M. Hjorth-Jensen, J. Rekstad, S. Siem, A. Schiller, and D. J. Dean, Phys. Rev. C **68**, 034311 (2003).

85. A. Schiller, A. Bjerve, M. Guttormsen, M. Hjorth-Jensen, F. Ingebretsen, E. Melby, S. Messelt, J. Rekstad, S. Siem, and S. W. Odegard, Phys. Rev. C **63**, 021306 (2001).

86. U. Agvaanluvsan, A. Schiller, J. A. Becker, L. A. Bernstein, P. E. Garrett, M. Guttormsen, G. E. Mitchell, J. Rekstad, S. Siem, A. Voinov, and W. Younes, Phys. Rev. C **70**, 054611 (2004).

87. A. Bürger, A. C. Larsen, S. Hilaire, M. Guttormsen, S. Harissopulos, M. Kmiecik, T. Konstantinopoulos, M. Krticka, A. Lagoyannis, T. Loennroth, K. Mazurek, M. Norrby, H. T. Nyhus, G. Perdikakis, S. Siem, A. Spyrou, and N. U. H. Syed, Phys. Rev. C **85**, 064328 (2012).

88. A. C. Larsen, M. Guttormsen, R. Chankova, F. Ingebretsen, T. Loennroth, S. Messelt, J. Rekstad, A. Schiller, S. Siem, N. U. H. Syed, and A. Voinov, Phys. Rev. C **76**, 044303 (2007).

89. N. U. H. Syed, A. C. Larsen, A. Bürger, M. Guttormsen, S. Harissopulos, M. Kmiecik, T. Konstantinopoulos, M. Krticka, A. Lagoyannis, T. Lnnroth, K. Mazurek, M. Norby, H. T. Nyhus, G. Perdikakis, S. Siem, and A. Spyrou, Phys. Rev. C **80**, 044309 (2009).

90. M. Guttormsen, A. C. Larsen, A. Bürger, A. Goergen, S. Harissopulos, M. Kmiecik, T. Konstantinopoulos, M. Krticka, A. Lagoyannis, T. Loennroth, K. Mazurek, M. Norrby, H. T. Nyhus, G. Perdikakis, A. Schiller, S. Siem, A. Spyrou, N. U. H. Syed, H. K. Toft, G. M. Tveten, and A. Voinov, Phys. Rev. C **83**, 014312 (2011).

91. A. C. Larsen, R. Chankova, M. Guttormsen, F. Ingebretsen, S. Messelt, J. Rekstad, S. Siem, N. U. H. Syed, S. W. Oedegard, T. Loennroth, A. Schiller, and A. Voinov, Phys. Rev. C **73**, 064301 (2006).

92. K.-H. Schmidt and B. Jurado, Phys. Rev. C **86**, 044322 (2012).

93. K.-H. Schmidt and B. Jurado, Phys. Rev. Lett. **104**, 212501 (2010).

94. K.-H. Schmidt and B. Jurado, Phys. Rev. C **83**, 061601 (2011).

95. A. A. Naqvi, F. Käppeler, F. Dickmann, and R. Müller, Phys. Rev. C **34**, 218 (1986).

96. R. Müller, A. A. Naqvi, F. Käppeler, and F. Dickmann, Phys. Rev. C **29**, 885 (1984).

97. V. V. Malinovskij, V. G. Vorob'eva, and B. D. Kuz'minov, Report INDC(CCP)-239, IAEA, Vienna, Austria, 1985.

98. R. W. Mills, *Fission product yield evaluation*, PhD thesis, University of Birmingham, 1995.

99. M. B. Chadwick, M. Herman, P. Oblozinsky, M. E. Dunn, Y. Danon, A. C. Kahler, D. L. Smith, B. Pritychenko, G. Arbanas, R. Arcilla, R. Brewer, D. A. Brown, R. Capote, A. D. Carlson, Y. S. Cho, H. Derrien, K. Guber, G. M. Hale, S. Hoblit, S. Holloway, T. D. Johnson, T. Kawano, B. C. Kiedrowski, H. Kim, S. Kunieda, N. M. Larson, L. Leal, J. P. Lestone, R. C. Little, E. A. McCutchan, R. E. MacFarlane, M. MacInnes, C. M. Mattoon, R. D. McKnight, S. F. Mughabghab, G. P. A. Nobre, G. Palmiotti, A. Palumbo, M. T. Pigni, V. G. Pronyaev, R. O. Sayer, A. A. Sonzogni, N. C. Summers, P. Talou, I. J. Thompson, A. Trkov, R. L. Vogt, S. C. van der Marck, A. Wallner, M. C. White, D. Wiarda, and P. G. Young, Nucl. Data Sheet **112**, 2887 (2011).

100. B. Jurado and K.-H. Schmidt J. Phys. G: Nucl. Part. Phys. **42**, 055101 (2015).
101. M. Dahlinger, D. Vermeulen, and K.-H. Schmidt, Nucl. Phys. A **376**, 94 (1982).
102. W. D. Myers and W. J. Swiatecki, Ann. Phys. **84**, 186 (1974).